



Article

Efficient Photodegradation of Rhodamine B by Fiber-like Nitrogen-Doped TiO₂/Ni(OH)₂ Nanocomposite under Visible Light Irradiation

Huan Wang^{1,2}, Mingxuan Dong², Baorui Shao², Yaodan Chi^{1,*}, Chao Wang¹, Sa Lv¹ , Ran Duan¹, Boqi Wu¹ and Xiaotian Yang^{1,3,*}

¹ Key Laboratory for Comprehensive Energy Saving of Cold Regions Architecture of Ministry of Education, Jilin Jianzhu University, Changchun 130118, China; wanghuan@jlju.edu.cn (H.W.); wangchao@jlju.edu.cn (C.W.); lvsa82@163.com (S.L.); 18186880816@163.com (R.D.); xiancaitang@sina.com (B.W.)

² Department of Materials Science, Jilin Jianzhu University, Changchun 130118, China; dong990816@163.com (M.D.); br13180828503@163.com (B.S.)

³ Department of Chemistry, Jilin Normal University, Siping 136000, China

* Correspondence: chiyaodan@jlju.edu.cn (Y.C.); hanyxt@163.com (X.Y.); Tel.: +86-0431-84566327 (Y.C.); +86-0434-3295002 (X.Y.)

Abstract: N-TiO₂/Ni(OH)₂ nanofiber was successfully prepared by combining the electrospinning and solvothermal method. It has been found that under visible light irradiation, the as-obtained nanofiber exhibits excellent activity for the photodegradation of rhodamine B, and the average degradation rate reaches 3.1%/min⁻¹. Further insight investigations reveal that such a high activity was mainly due to the heterostructure-induced increase in the charge transfer rate and separation efficiency.

Keywords: photocatalysis; charge transfer; heterostructure



Citation: Wang, H.; Dong, M.; Shao, B.; Chi, Y.; Wang, C.; Lv, S.; Duan, R.; Wu, B.; Yang, X. Efficient Photodegradation of Rhodamine B by Fiber-like Nitrogen-Doped TiO₂/Ni(OH)₂ Nanocomposite under Visible Light Irradiation. *Micromachines* **2023**, *14*, 870. <https://doi.org/10.3390/mi14040870>

Academic Editor: Sadia Ameen

Received: 23 March 2023

Revised: 12 April 2023

Accepted: 14 April 2023

Published: 18 April 2023



Copyright: © 2023 by the authors. Licensee MDPI, Basel, Switzerland. This article is an open access article distributed under the terms and conditions of the Creative Commons Attribution (CC BY) license (<https://creativecommons.org/licenses/by/4.0/>).

1. Introduction

Back in 2001, Asahi et al. [1,2] identified that the tactic of non-metal-doping can narrow the bandgap of TiO₂ (anatase, 3.2 eV). Both experimental results and the relevant density functional theory (DFT) theoretical calculations revealed that nitrogen doping could significantly extend the absorption range of TiO₂ into the visible region. Since then, numerous investigations focus on non-metal-doped (N, S, P, B) TiO₂ photocatalysts [3,4]. Through the non-metallic dopants and their combinations, the corresponding photocatalytic activity of derived TiO₂ could be improved, thus exhibiting outstanding photocatalytic performances in various applications, such as photocatalytic water splitting [5,6], CO₂ reduction [7,8], removal of organic compounds [9,10], sterilization [11], and anti-viral applications [12]. Owing to these excellent properties, N-doped TiO₂ and cocatalyst-supported TiO₂ have been commercialized and widely used in many practical applications [13]. However, the photocatalytic reaction rate of N-doped TiO₂ is still very low, which is believed to be caused by the following two reasons: one is its weak absorption in the visible range, while the other is the limited rate of the photocatalytic reactions by the nitrogen-induced oxygen vacancies, which is supposed to act as the carrier traps and/or recombination centers.

To enhance the photocatalytic performance of nitrogen-doped TiO₂ (N-TiO₂) in the visible range, tremendous efforts have been devoted to it during the past decades [14–16]. It has been revealed that transition metal nickel hydroxide and NiS could act as cocatalysts to significantly strengthen the photocatalytic activity of TiO₂, which is believed to be attributed to the inhibition of charge carriers' recombination [17–19]. Zhang et al. [20] prepared three-dimensional flower-like TiO₂@Ni(OH)₂ core-shell heterostructures, exhibiting a six-fold activity enhancement for hydrogen photogeneration. Meng et al. [21] synthesized a hierarchical TiO₂/Ni(OH)₂ composite photocatalyst via decorating Ni(OH)₂ nanosheets

on the electrospun TiO₂ nanofibers by a simple wet method, and the results indicate that, compared to pristine TiO₂ fibers, its activity of CO₂ photoreduction was significantly improved, which was ascribed to the increased charge separation efficiency and higher CO₂ capture capacity owing to the presence of Ni(OH)₂. Chen et al. [22] reported the construction of a photo-supercapacitor with high specific capacitance and ultra-fast charge-discharge response, in which TiO₂ was used as a photoelectric conversion material and Ni(OH)₂ was used as an energy storage material in the TiO₂/Ni(OH)₂ composite material, offering a simple fabrication process for efficient direct solar energy storage. These findings inspired us to develop a heterojunction between N-TiO₂ and nickel hydroxide to increase the charge separation efficiency thereby improving its corresponding photocatalytic activity.

To our knowledge, only a few studies were focused on the photocatalytic applications of N-TiO₂/Ni(OH)₂ composite. In this work, we first prepared N-TiO₂ nanofibers by electrospinning technique followed by decoration of Ni(OH)₂ via the hydrothermal method to obtain the high-quality N-TiO₂/Ni(OH)₂ heterostructures. The designated composite exhibits a much-enhanced photocatalytic ability for the degradation of rhodamine B (RhB) compared to N-TiO₂ under visible light irradiation. Further detailed analyses reveal the relevant enhanced activity is ascribed to the increased charge separation efficiency induced by the delicate heterostructure.

2. Experimental Section

2.1. Chemicals and Reagents

Acetic acid (99.5%), butyl titanate (99.0%), ethanol (99.0%), urea (99.0%), polyvinylpyrrolidone (99.0%), Rhodamine B (99.0%), nickel nitrate hexahydrate (99.0%), and hexamethylenetetramine (99.0%) were purchased from Shanghai Aladdin Biochemical Technology Co., Ltd. (Shanghai, China). All chemicals were used as received without further purification.

2.2. Synthesis of Ni(OH)₂ Nanosheets

N-TiO₂ nanofibers were prepared by the electrospinning method according to the previous work [23]. Typically, 5 mL of acetic acid and 5 mL of butyl titanate were added into 10 mL ethanol under vigorous stirring at room temperature (RT). After ~10 min., 0.2 g of urea was introduced, followed by another 20 min stirring. Meanwhile, another solution was obtained by introducing 1.5 g of polyvinylpyrrolidone into 10 mL ethanol. Then, the two above solutions were homogeneously mixed and further heated at 70 °C for 1 h under vigorous stirring to obtain the precursor solution for electrospinning. At a static voltage of 15 kV, a capillary tube with an inner diameter of 0.5 mm at a 15 cm distance from the collector was used to prepare the electrospun film. The flow rate was set at 1 mL/h. Afterward, the fiber film was peeled off and placed in a crucible that was sealed with tin foil and kept at 550 °C for 3 h in a muffle furnace to obtain N-TiO₂ fibers. For comparison, TiO₂ nanofibers were prepared by a similar procedure and the only exception is without introducing urea.

2.3. Preparation of N-TiO₂/Ni(OH)₂ Nanocomposite

A total of 100 mg of the as-prepared N-TiO₂ nanofibers were added into 40 mL ultra-pure water followed by sonication for 10 min to obtain a homogeneous suspension. Next, 3.1 mg nickel nitrate hexahydrate and 1.7 mg hexamethylenetetramine were introduced and the corresponding solution was further stirred for 1 h at RT. Then, the solution was transferred to the Teflon-lined autoclave and heated at 120 °C for another 6 h. The obtained precipitation was alternatively washed with ethanol and water several times and subsequently dried in a vacuum oven at 80 °C for 4 h. Samples with 0.5 and 1.5 wt% Ni(OH)₂ contents were prepared by the same protocol with different amounts of nickel nitrate hexahydrate and hexamethylenetetramine introduced.

2.4. Characterization

The crystal structure of samples was investigated on an X-ray diffractometer (Rigaku D/Max 2550, Japan Rigaku Co., Ltd., Tokyo, Japan) at 40 kV and 40 mA with copper $K\alpha$ radiation ($\lambda = 0.154056$ nm). The morphological and structural information was characterized via field-emission scanning electron microscopy (SEM, JSM-7610F, Tokyo, Japan) and transmission electron microscopy (TEM, Tecnai G2 F20 S-TWIN, FEI, Valley City, ND, USA). X-ray photoelectron spectroscopy (XPS) measurements were recorded by a photoelectron spectrometer (ESCALAB MKII, VG Scientific, Waltham, MA, USA). The relevant photoluminescence results were obtained on an FLS-1000 fluorescence spectrophotometer (Edinburgh Instruments Ltd., Livingston, UK). The transient photocurrent signals were measured by an electrochemical workstation (CHI-660, CH Instruments, Austin, TX, USA). UV-Vis diffuse reflectance spectra of the samples, and the absorbance of Rh B solution was measured on a Shimadzu-2600 spectrophotometer (Shimadzu, Kyoto, Japan).

2.5. Measurement of Photocatalytic Reactions

The RhB photodegradation experiments were performed in a glass flask. Typically, 25 mg of the relevant photocatalyst was dispersed into a 100 mL Rh B aqueous solution (10 mg/L). Before the photoreaction, the solution was stirred for 30 min in dark to exclude the adsorption effect of the sample. Then, the solution was illuminated by a 300-W Xenon lamp with a filter (>420 nm). A total of 2 mL of the solution was taken at regular intervals (30 min), then subjected to UV-Vis measurements after filtrating the photocatalyst.

3. Results

The crystal structural information of TiO_2 , N- TiO_2 , and N- $\text{TiO}_2/\text{Ni}(\text{OH})_2$ nanofibers were obtained by X-ray diffraction (XRD) technique. As shown (Figure 1), for TiO_2 , the clear diffraction peaks at $2\theta = 25.2^\circ, 37.8^\circ, 47.8^\circ, 55.2^\circ, 62.7^\circ, 68.9^\circ, 75.1^\circ,$ and 82.6° ascribed to (101), (004), (200), (105), (204), (116), and (215) crystal planes of anatase (JCPDS card number 21-1272) were observed, respectively. Meanwhile, peaks at $2\theta = 27.4^\circ, 36.1^\circ,$ and 41.1° , which is consistent with the (110), (101), and (111) crystal planes of rutile, respectively, TiO_2 (JCPDS card number 21-1276) are also detected. The results demonstrate that under the current calcination condition, the obtained TiO_2 nanofibers are in the mixed phase of anatase and rutile. Interestingly, when nitrogen is introduced into TiO_2 , the rutile phase of TiO_2 seems to be significantly inhibited. Furthermore, for N- $\text{TiO}_2/\text{Ni}(\text{OH})_2$ nanocomposite, no peak belonging to $\text{Ni}(\text{OH})_2$ was observed, which is considered to be owing to the low $\text{Ni}(\text{OH})_2$ content [18].

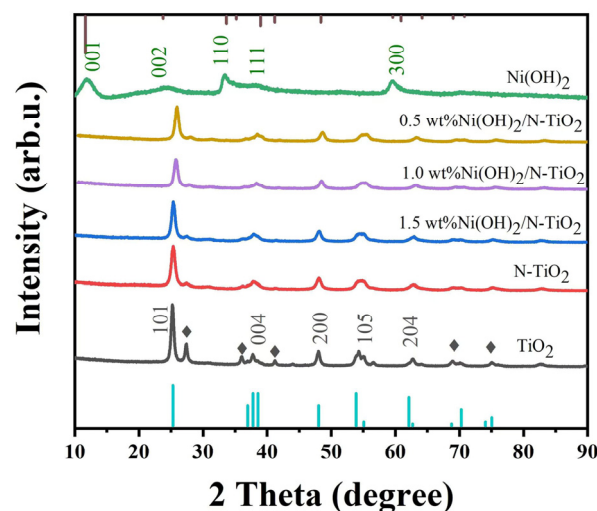


Figure 1. X-ray diffraction (XRD) patterns of TiO_2 , N- TiO_2 , $\text{Ni}(\text{OH})_2$, and N- $\text{TiO}_2/\text{Ni}(\text{OH})_2$ with different amount of $\text{Ni}(\text{OH})_2$. The rectangle indicates the rutile phase of TiO_2 .

The morphological and structural information of the sample was obtained by SEM and TEM measurements. Figure 2a displays the SEM result of TiO₂ nanofibers. It is seen that the TiO₂ was in a fibrous structure with a diameter of ~500 nm and length over 10 μm, while the introduction of nitrogen did not induce any observable morphological change (Figure 2b). Further decoration of Ni(OH)₂ onto N-TiO₂ nanofibers could induce the two-dimensional structural growth on the surface of the corresponding samples, (Figure 2c), which manifests the successful deposition of Ni(OH)₂. TEM image of the N-TiO₂/1.0 wt% Ni(OH)₂ nanofibers indicates the diameter of the relevant sample in ~500 nm (Figure 2d), and higher magnification TEM result clearly demonstrates a 50-nm-thick layer was homogeneously coated onto the outside surface of the N-TiO₂ fibers, which is considered to be Ni(OH)₂ (Figure 2e). Furthermore, HRTEM measurement confirms our assumption. As is shown (Figure 2f), the clear granular nanostructure ascribed to (110) crystal plane of Ni(OH)₂ was found in the corresponding outside layer area of the sample, and the green circle represents Ni(OH)₂ nanocrystalline particles in Figure 2f.

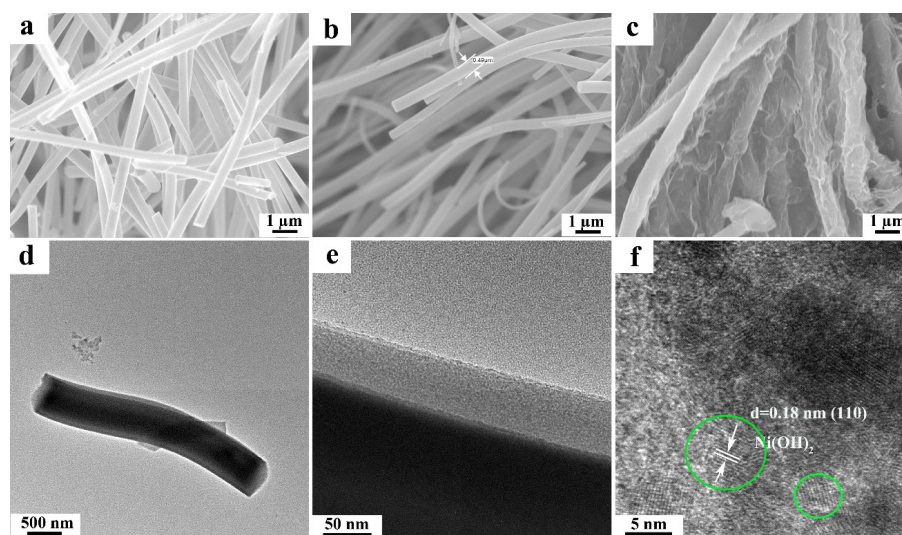


Figure 2. SEM, TEM, and high-resolution TEM (HRTEM) images of (a) TiO₂ fibers, (b) N-TiO₂ fibers, and (c–f) N-TiO₂/1.0 wt% Ni(OH)₂ composite fibers.

To acquire the chemical state of each element in the samples, XPS measurements were performed. Figure 3 shows the high-resolution Ti 2p, O 1s, N 1s, and Ni 2p XPS spectra of the N-TiO₂/1.0 wt% Ni(OH)₂. As is shown for Ti 2p, peaks at 458.5 and 464.3 eV could be ascribed to Ti 2p_{3/2} and Ti 2p_{1/2} of TiO₂, respectively, indicating the existence of Ti⁴⁺ in the sample [24–26]; while for O 1s, signals of lattice oxygen (titanium–oxygen–titanium, 529.7 eV) and hydroxyl oxygen (Ti–OH and Ni–OH, 531.4 eV) are observed [27] (Figure 3b). A weak characteristic peak (N1s) at 399.9 eV attributes to the signal combination of weakly charged nitrogen species with C, H, or O atoms [28] (Figure 3c), and demonstrates the successful diffusion of nitrogen into the TiO₂ lattice at interstitial positions [29,30]. It is noted that nitrogen had a weak positive charge in the Ni 2p region (Figure 3d) due to the bonding with O atoms of TiO₂ [30–32]. In addition, the peaks at 855.3 and 873.0 eV correspond to Ni 2p_{3/2} and Ni 2p_{1/2}, respectively, indicating the existence of nickel hydroxide [33]. In addition, the two shoulder peaks were ascribed to the satellite peaks of Ni 2p_{3/2} and Ni 2p_{1/2} in the vicinity of 861.7 and 880.3 eV, respectively [20].

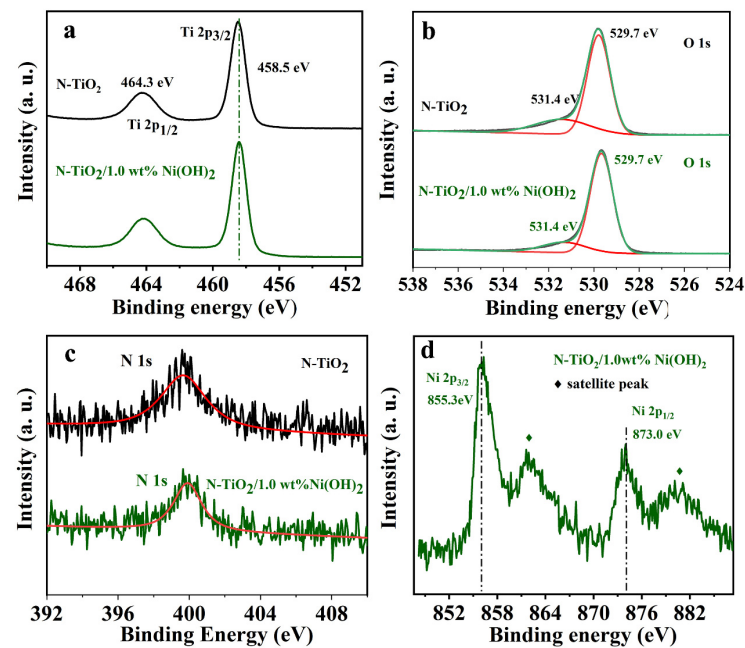


Figure 3. XPS spectra of (a) Ti 2p, (b) O 1s, (c) N 1s, and (d) Ni 2p of N-TiO₂/1.0 wt% Ni(OH)₂ nanofibers. The red lines in (b,c) are the fitted curves of the corresponding data.

The absorption property of different samples was measured by UV-Vis diffuse reflectance absorption spectroscopy. As indicated (Figure 4), Ni(OH)₂ control sample exhibits an obvious absorption at 450 and 600–800 nm, which is due to the d–d transition of Ni [34]. In addition, compared to TiO₂, the absorption of N-TiO₂ and different N-TiO₂/Ni(OH)₂ samples in the visible region are significantly enhanced. It should be noted that, in the range of 400–550 nm, the absorption intensity of N-TiO₂/Ni(OH)₂ nanofibers is increased with the increase in Ni(OH)₂ content.

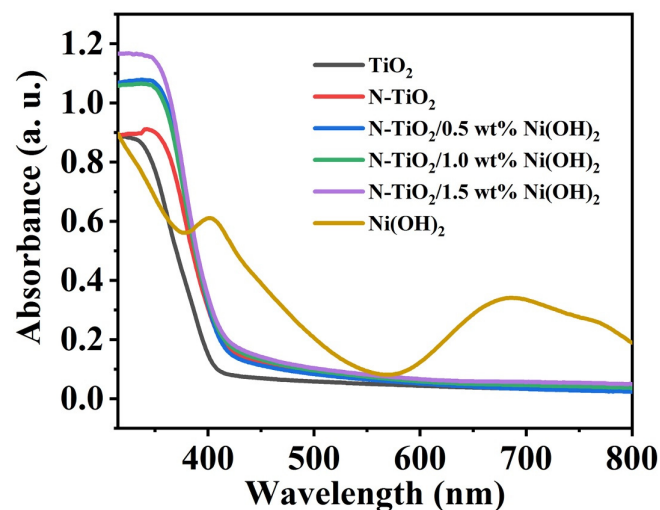


Figure 4. UV-Vis diffuse reflectance absorption spectra of Ni(OH)₂, TiO₂, N-TiO₂, N-TiO₂/Ni(OH)₂ with different Ni(OH)₂ contents, respectively.

The photocatalytic activity on the degradation of RhB of different samples was then evaluated. As shown (Figure 5a), all the employed samples exhibit the similar physical adsorption property for RhB. However, interestingly, once illuminated, all the N-TiO₂/Ni(OH)₂ nanocomposites show a much higher ability for the photodegradation of RhB compared to that of a relevant single component. Especially, N-TiO₂/Ni(OH)₂ nanocomposite possesses the best performance, and ~97% of RhB would be photodegraded

in 90 min. To illustrate the decomposition rate more clearly, the Langmuir-Hinshelwood kinetics equation was employed [35]. As shown in Figure 5b, the activities of all the nanocomposites were higher than those of a single component, indicating an apparent synergistic effect between N-TiO₂ and Ni(OH)₂, which could also be reflected by the rate constant (Figure 5c). Our results unambiguously manifest the vital role of forming the heterostructure for significantly enhancing the RhB photodegradation ability. Further optimization of the addition of Ni(OH)₂ in the composite showed that when the amount of Ni(OH)₂ in the composite is 1.0-wt%, the best performance of 0.0310 min⁻¹ could be achieved (Figure 5b), which was comparable to the recent benchmark test results (Table 1).

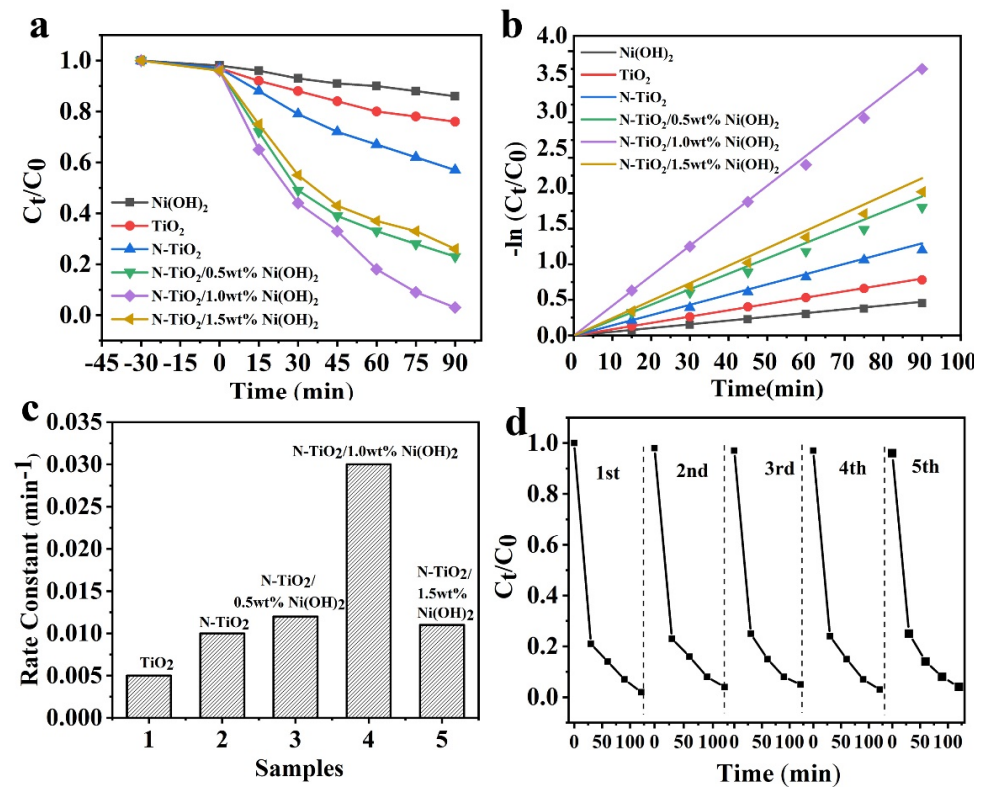


Figure 5. (a) Photodegradation of RhB for TiO₂, N-TiO₂, Ni(OH)₂, and N-TiO₂/Ni(OH)₂ of different Ni(OH)₂ contents under the irradiation of visible-light (>420 nm); (b) Natural logarithm degradation curves of different samples; (c) Rate constants (k_R) of different samples for photodegradation of RhB; (d) five consecutive photodegradation curves of RhB over N-TiO₂/1.0-wt% Ni(OH)₂ under the visible light irradiation.

Table 1. Comparison of the catalytic performance of N-TiO₂/Ni(OH)₂ with the previously reported data for the reduction in organic dyes of Rh B.

Material Used	Light Used	Dye Degradation	K _{app} (min ⁻¹)	Removal (%) / 30 min	Ref.
N-TiO ₂ /Ni(OH) ₂	visible light	RhB	0.0310	60%	This work
Ni(OH) ₂	UV-visible	RhB	0.0130	/	[36]
NiO-ZnO	UV-visible	RhB	0.0302	50	[37]
NixOy/TiO ₂	UV-visible	RhB	0.0349	56.5	[38]
Ni/NiO/TiO ₂	UV-visible	RhB	/	35	[39]
NiO/BVO	UV-visible	RhB	/	40	[40]

The stability of photocatalyst is a critical issue for the potential real application. Hence, the relevant stability of N-TiO₂/1.0-wt% Ni(OH)₂ was evaluated (Figure 5d). After each round of photocatalytic reaction, the sample was collected via centrifugation and washed with ultrapure water several times before further usage. As shown, only a slight activity decrease (~3.7%) was observed after five cycles demonstrating its excellent stability for long-term use.

To elucidate the underlying mechanism of the heterostructure-induced photocatalytic activity enhancement, photoluminescence (PL) measurements were first employed. As shown in Figure 6a, N-TiO₂ gives an obvious PL emission in the range of 400–550 nm, while for that of Ni(OH)₂, hardly any PL signal could be observed. Interestingly, for the nanocomposite sample, the relevant PL intensity is gradually decreased with the gradual increase in Ni(OH)₂ content, which is considered to be ascribed to charge transfer from N-TiO₂ to Ni(OH)₂ [35]. To further verify the separation and migration behavior of charge carriers, photocurrent response tests were performed. As shown in Figure 6b, all the composite samples give higher photocurrent responses than that of the N-TiO₂ or Ni(OH)₂, and N-TiO₂/1.0 wt% Ni(OH)₂ exhibits the highest response, which is consistent with the trend of their photocatalytic performance. This strongly signifies the introduction of Ni(OH)₂ is beneficial for increasing charge separation efficiency, and thus enhances the relevant photocatalytic activity.

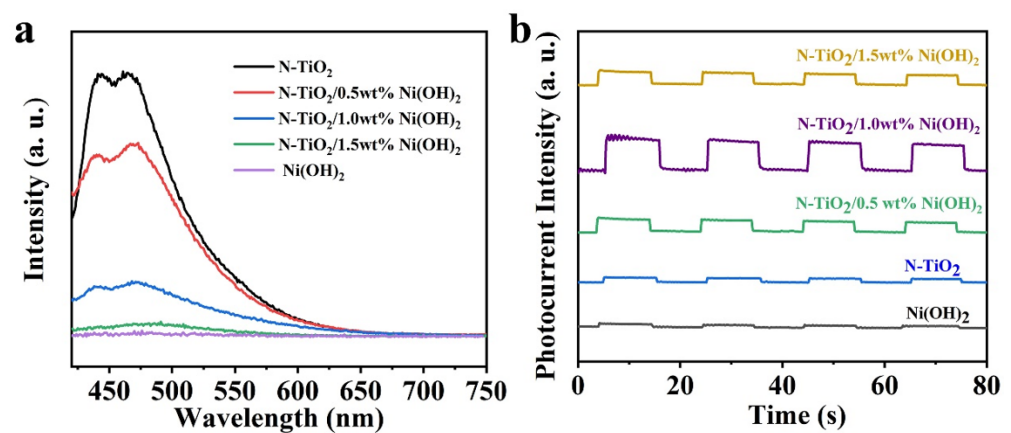


Figure 6. (a) PL spectra and (b) photocurrent response (>420 nm) of N-TiO₂, Ni(OH)₂, and N-TiO₂/Ni(OH)₂ with different Ni(OH)₂ content, respectively.

Based on the above results, the plausible underlying mechanism for the enhanced photocatalytic activity of N-TiO₂/Ni(OH)₂ composite has been proposed (Figure 7). After the absorption of the incident light, both N-TiO₂ and Ni(OH)₂ were excited. Thereafter, the electrons and holes are photogenerated in each component, and electrons are excited into the conduction band (CB) while the holes are left at the valence band (VB). Owing to the potential of Ni²⁺/Ni (0.23 eV) being slightly lower than that of anatase TiO₂ (~0.26 eV), photogenerated electrons will transfer from CB of TiO₂ into CB of Ni(OH)₂, while holes remain in VB of TiO₂. This will significantly promote charge separation and inhibit the recombination of photogenerated electrons and holes. Subsequently, electrons could react with adsorbed oxygen to generate superoxide free radicals. It is noted the formation of free radicals can not only effectively inhibit electron-hole recombination, but also destroy the bonds of RhB and therefore degrade them, which finally exhibits enhanced photocatalytic activity.

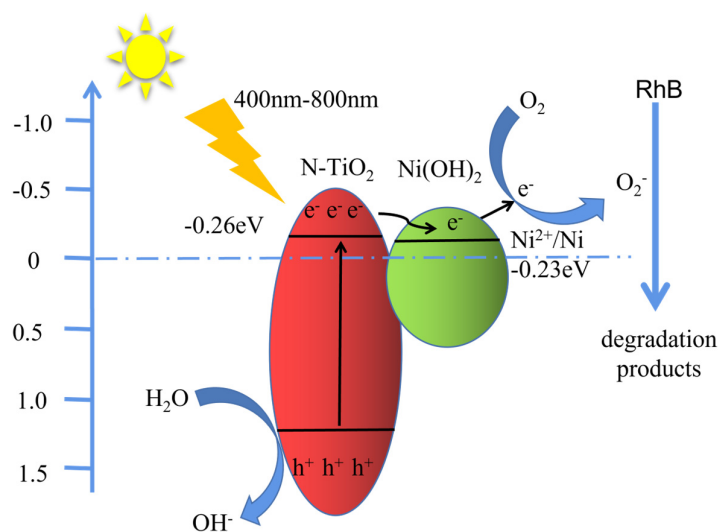


Figure 7. Schematic diagram of the mechanism of photocatalytic degradation of Rh B by $\text{Ni}(\text{OH})_2/\text{N-TiO}_2$ under visible light irradiation.

4. Conclusions

In this work, the heterostructured $\text{N-TiO}_2/\text{Ni}(\text{OH})_2$ nanofibers were successfully constructed and further applied for the enhanced photodegradation of RhB compared to that of N-TiO_2 under visible light irradiation (>420 nm). Our results indicate that the elaborated design could significantly enhance the corresponding photocatalytic activity and the one with 1.0 wt% $\text{Ni}(\text{OH})_2$ exhibits the best performance. Further detailed investigations revealed that the enhanced activity is mainly ascribed to the efficient charge transfer and separation in N-TiO_2 induced by the integration of $\text{Ni}(\text{OH})_2$. It is anticipated that our tactics and results would be beneficial for the future design of high-performance photocatalysts.

Author Contributions: Conceptualization, H.W. and M.D.; methodology, H.W. and B.S.; validation, Y.C. and C.W.; formal analysis, H.W. and S.L.; investigation, H.W. and X.Y.; writing—original draft preparation, H.W. and R.D.; writing—review and editing, H.W., B.W., Y.C. and X.Y.; visualization, M.D. and B.S.; supervision, X.Y. All authors have read and agreed to the published version of the manuscript.

Funding: This research was funded by the science and technology development project of Jilin province, China (No. 20230508059RC, No. 20210203098SF, and No. 20210203021SF), the financial support from Key Laboratory for Comprehensive Energy Saving of Cold Regions Architecture of Ministry of Education (No. JLZHKF022021008).

Data Availability Statement: The data presented in this study are available on request from the corresponding author.

Conflicts of Interest: The authors declare no conflict of interest.

References

- Asahi, R.; Morikawa, T.; Ohwaki, T.; Aoki, K.; Taga, Y. Visible-Light Photocatalysis in Nitrogen-Doped Titanium Oxides. *Science* **2001**, *293*, 269–271. [[CrossRef](#)]
- Morikawa, T.; Asahi, R.; Ohwaki, T.; Aoki, K.; Taga, Y. Band-Gap Narrowing of Titanium Dioxide by Nitrogen Doping. *Jpn. J. Appl. Phys.* **2001**, *40*, L561. [[CrossRef](#)]
- Devi, L.G.; Kavitha, R. A review on nonmetal ion doped titania for the photocatalytic degradation of organic pollutants under UV/solar light: Role of photogenerated charge carrier dynamics in enhancing the activity. *Appl. Catal. B Environ.* **2013**, *140–141*, 559–587. [[CrossRef](#)]
- Yang, Y.; Zhong, H.; Tian, C. Photocatalytic mechanisms of modified titania under visible light. *Res. Chem. Intermed.* **2011**, *37*, 91–102. [[CrossRef](#)]
- Reddy, P.A.K.; Reddy, P.V.L.; Kim, K.-H.; Kumar, M.K.; Manvitha, C.; Shimn, J.-J. Novel Approach for the Synthesis of Nitrogen-Doped Titania with Variable Phase Composition and Enhanced Production of Hydrogen under Solar Irradiation. *J. Ind. Eng. Chem.* **2017**, *53*, 253–260. [[CrossRef](#)]

6. Preethi, L.K.; Antony, R.P.; Mathews, T.; Loo, S.C.J.; Wong, L.H.; Dash, S.; Tyagi, A.K. Nitrogen Doped Anatase-Rutile Heterostructured Nanotubes for Enhanced Photocatalytic Hydrogen Production: Promising Structure for Sustainable Fuel Production. *Int. J. Hydrog. Energ.* **2016**, *41*, 5865–5877. [[CrossRef](#)]
7. Akple, M.S.; Low, J.; Qin, Z.; Wageh, S.; Al-Ghamdi, A.A.; Yu, J.; Liu, S. Nitrogen-Doped TiO₂ Microsheets with Enhanced Visible Light Photocatalytic Activity for CO₂ Reduction. *Chin. J. Catal.* **2015**, *36*, 2127–2134. [[CrossRef](#)]
8. Delavari, S.; Amin, N.A.S.; Ghaedi, M. Photocatalytic Conversion and Kinetic Study of CO₂ and CH₄ over Nitrogen-doped Titania Nanotube Arrays. *J. Clean. Prod.* **2016**, *111*, 143–154. [[CrossRef](#)]
9. Kamaludin, R.; Othman, M.H.D.; Kadir, S.H.S.A.; Ismail, A.F.; Rahman, M.A.; Jaafar, J. Visible-Light-Driven Photocatalytic N-doped TiO₂ for Degradation of Bisphenol A (BPA) and Reactive Black 5 (RB5) Dye. *Water Air Soil Pollut.* **2018**, *229*, 363. [[CrossRef](#)]
10. Le, P.; Hieu, L.; Lam, T.-N.; Hang, N.; Truong, N.; Tuyen, L.; Phong, P.; Leu, J. Enhanced Photocatalytic Performance of Nitrogen-doped TiO₂ Nanotube Arrays Using a Simple Annealing Process. *Micromachines* **2018**, *9*, 618. [[CrossRef](#)]
11. Ananpattarachai, J.; Boonto, Y.; Kajitvichyanukul, P. Visible Light Photocatalytic Antibacterial Activity of Ni-doped and N-doped TiO₂ on Staphylococcus aureus and Escherichia coli Bacteria. *Environ. Sci. Pollut. Res.* **2015**, *23*, 4111–4119. [[CrossRef](#)] [[PubMed](#)]
12. Asahi, R.; Hiroshi, T.; Vequizo, J.-M.; Yamakata, A. Improvement of photocatalytic activity under visible-light irradiation by heterojunction of Cu ion loaded WO₃ and Cu ion loaded N-TiO₂. *Appl. Catal. B Environ.* **2019**, *248*, 249–254.
13. Asahi, R.; Morikawa, T.; Irie, H.; Ohwaki, T. Nitrogen-Doped Titanium Dioxide as Visible-Light-Sensitive Photocatalyst: Designs, Developments, and Prospects. *Chem. Rev.* **2014**, *114*, 9824–9852. [[CrossRef](#)]
14. Zhao, Y.; Qiu, X.; Burda, C. The Effects of Sintering on the Photocatalytic Activity of N-Doped TiO₂ Nanoparticles. *Chem. Mater.* **2008**, *20*, 2629–2636. [[CrossRef](#)]
15. Kumar, M.P.; Jagannathan, R.; Ravichandran, S. Photoelectrochemical System for Unassisted High-Efficiency Water-Splitting Reactions Using N-Doped TiO₂ Nanotubes. *Energy Fuels* **2020**, *34*, 9030–9036. [[CrossRef](#)]
16. Zhang, J.; Li, Y.; Li, L.; Li, W.; Yang, C. Dual Functional N-Doped TiO₂-Carbon Composite Fibers for Efficient Removal of Water Pollutants. *ACS Sustain. Chem. Eng.* **2018**, *6*, 12893–12905. [[CrossRef](#)]
17. Ong, W.L.; Ng, S.W.L.; Zhang, C.; Hong, M.; Ho, G.W. 2D hydrated layered Ni(OH)₂ structure with hollow TiO₂ nanocomposite directed chromogenic and catalysis capabilities. *J. Mater. Chem. A* **2016**, *4*, 13307–13315. [[CrossRef](#)]
18. Yu, J.; Hai, Y.; Cheng, B. Enhanced Photocatalytic H₂-Production Activity of TiO₂ by Ni(OH)₂ Cluster Modification. *J. Phys. Chem. C* **2011**, *115*, 4953–4958. [[CrossRef](#)]
19. Luo, Y.; Dong, J.; Jiang, Z.; Zhan, X.; Li, Y.; Wang, C. β-Ni(OH)₂/NiS/TiO₂ 3D flower-like p-n-p heterostructural photocatalysts for high-efficiency removal of soluble anionic dyes and hydrogen releasing. *Opt. Mater.* **2021**, *114*, 110951. [[CrossRef](#)]
20. Zhang, W.; Zhang, H.; Xu, J.; Zhuang, H.; Long, J. 3D flower-like heterostructured TiO₂@Ni(OH)₂ microspheres for solar photocatalytic hydrogen production. *Chin. J. Catal.* **2019**, *40*, 320–325. [[CrossRef](#)]
21. Meng, A.; Wu, S.; Cheng, B.; Yu, J.; Xu, J. Hierarchical TiO₂/Ni(OH)₂ composite fibers with enhanced photocatalytic CO₂ reduction performance. *J. Mater. Chem. A* **2018**, *6*, 4729–4736. [[CrossRef](#)]
22. Chen, P.; Cao, C.; Ding, C.; Yin, Z.; Qi, S.; Guo, J.; Zhang, M.; Sun, Z. One-body style photo-supercapacitors based on Ni(OH)₂/TiO₂ heterojunction array: High specific capacitance and ultra-fast charge/discharge response. *J. Power Sources* **2022**, *521*, 230920. [[CrossRef](#)]
23. Gao, M.; Sheng, W.; Zhuang, Z.; Fang, Q.; Gu, S.; Jiang, J.; Yan, Y. Efficient Water Oxidation Using Nanostructured α-Nickel-Hydroxide as an Electrocatalyst. *J. Am. Chem. Soc.* **2014**, *136*, 7077–7084. [[CrossRef](#)]
24. Wang, H.; Xiao, L.; Wang, C.; Lin, B.; Lv, S.; Chu, X.F.; Chi, Y.D.; Yang, X.T. Pd/TiO₂ Nanospheres with Three-dimensional Hyperstructure for Enhanced Photodegradation of Organic Dye. *Chem. Res. Chin. Univ.* **2019**, *35*, 667–673. [[CrossRef](#)]
25. Reddy, N.L.; Cheralathan, K.K.; Kumari, V.D.; Neppolian, B.; Venkatakrishnan, S.M. Photocatalytic Reforming of Biomass Derived Crude Glycerol in Water: A Sustainable Approach for Improved Hydrogen Generation Using Ni(OH)₂ Decorated TiO₂ Nanotubes under Solar Light Irradiation. *ACS Sustain. Chem. Eng.* **2018**, *6*, 3754–3764. [[CrossRef](#)]
26. Cipagauta-Díaz, S.; Estrella-González, A.; Navarrete-Magaña, M.; Gómez, R. N doped-TiO₂ coupled to BiVO₄ with high performance in photodegradation of Ofloxacin antibiotic and Rhodamine B dye under visible light. *Catal. Today* **2022**, *394*, 445–457. [[CrossRef](#)]
27. Liu, F.; Xie, Y.; Yu, C.; Liu, X.; Dai, Y.; Liu, L.; Ling, Y. Novel hybrid Sr-doped TiO₂/magnetic Ni_{0.6}Zn_{0.4}Fe₂O₄ for enhanced separation and photodegradation of organics under visible light. *RSC Adv.* **2015**, *5*, 24056–24063. [[CrossRef](#)]
28. Kovalevskiy, N.; Selishchev, D.; Svintsitskiy, D.; Selishcheva, S.; Berezin, A.; Kozlov, D. Synergistic effect of polychromatic radiation on visible light activity of Ndoped TiO₂ photocatalyst. *Catal. Commun.* **2020**, *134*, 105841. [[CrossRef](#)]
29. Motlak, M.; Akhtar, M.S.; Barakat, N.A.M.; Hamza, A.M.; Yang, O.B.; Kim, H.Y. High-Efficiency Electrode Based on Nitrogen-Doped TiO₂ Nanofibers for Dye-Sensitized Solar Cells. *Electrochim. Acta* **2014**, *115*, 493–498. [[CrossRef](#)]
30. Liu, S.J.; Ma, Q.; Gao, F.; Song, S.H.; Gao, S. Relationship between N-doping induced point defects by annealing in ammonia and enhanced thermal stability for anodized titania nanotube arrays. *J. Alloys Compd.* **2012**, *543*, 71–78. [[CrossRef](#)]
31. Peng, F.; Cai, L.; Yu, H.; Wang, H.; Yang, J. Synthesis and characterization of substitutional and interstitial nitrogen-doped titanium dioxides with visible light photocatalytic activity. *J. Solid State Chem.* **2008**, *181*, 130–136. [[CrossRef](#)]
32. Chen, L.; Gu, Q.; Hou, L.; Zhang, C.; Lu, Y.; Wang, X.; Long, J. Molecular p-n heterojunction-enhanced visible light hydrogen evolution over a N-doped TiO₂ photocatalyst. *Catal. Sci. Technol.* **2017**, *7*, 2039–2049. [[CrossRef](#)]

33. Ran, J.; Yu, J.; Jaroniec, M. Ni(OH)₂ modified CdS nanorods for highly efficient visible-light-driven photocatalytic H₂ generation. *Green Chem.* **2011**, *13*, 2708–2713. [[CrossRef](#)]
34. Mao, L.; Ba, Q.; Jia, X.; Liu, S.; Liu, H.; Zhang, J.; Li, X.; Chen, W. Ultrathin Ni(OH)₂ nanosheets: A new strategy for cocatalyst design on CdS surfaces for photocatalytic hydrogen generation. *RSC Adv.* **2019**, *9*, 1260–1269. [[CrossRef](#)] [[PubMed](#)]
35. Mou, J.; Xu, Y.; Zhong, D.; Chang, H.; Xu, C.; Wang, H.; Shen, H. Efficient Visible-Light-Responsive Photocatalytic Fuel Cell with a ZnIn₂S₄/UiO-66/TiO₂/Ti Photoanode for Simultaneous RhB Degradation and Electricity Generation. *J. Electron. Mater.* **2022**, *51*, 6121–6133. [[CrossRef](#)]
36. Nagajyothi, P.C.; Deyarayapalli, K.C.; Tettey, C.O.; Vattikuti, S.V.P.; Shim, J. Eco-friendly green synthesis: Catalytic activity of nickel hydroxide nanoparticles. *Mater. Res. Express* **2019**, *6*, 055036. [[CrossRef](#)]
37. Shafi, A.; Ahmad, N.; Sultana, S.; Sabir, S.; Khan, M.Z. Ag₂S-Sensitized NiO–ZnO Heterostructures with Enhanced Visible Light Photocatalytic Activity and Acetone Sensing Property. *ACS Omega* **2019**, *4*, 12905–12918. [[CrossRef](#)]
38. Yang, M.; Lu, D.; Wang, H.; Wu, P.; Fang, P. A facile one-pot hydrothermal synthesis of two-dimensional TiO₂-based nanosheets loaded with surface-enriched Ni_xO_y nanoparticles for efficient visible-light-driven photocatalysis. *Appl. Surf. Sci.* **2019**, *467–468*, 124–134. [[CrossRef](#)]
39. Zhu, Q.; Liu, N.; Zhang, N.; Song, Y.; Stanislaus, M.S.; Zhao, C.; Yang, Y. Efficient photocatalytic removal of RhB, MO and MB dyes by optimized Ni/NiO/TiO₂ composite thin films under solar light irradiation. *J. Environ. Chem. Eng.* **2018**, *6*, 2724–2732. [[CrossRef](#)]
40. Peng, Y.; Cai, J.; Shi, Y.; Jiang, H.; Li, G. Thin p-type NiO nanosheet modified peanut-shaped monoclinic BiVO₄ for enhanced charge separation and photocatalytic activities. *Catal. Sci. Technol.* **2022**, *12*, 5162–5170. [[CrossRef](#)]

Disclaimer/Publisher’s Note: The statements, opinions and data contained in all publications are solely those of the individual author(s) and contributor(s) and not of MDPI and/or the editor(s). MDPI and/or the editor(s) disclaim responsibility for any injury to people or property resulting from any ideas, methods, instructions or products referred to in the content.